Energy & Environmental Science

PAPER

View Article Online
View Journal | View Issue

Cite this: *Energy Environ. Sci.*, 2025, **18**, 4120

High-performance inverted perovskite solar cells and modules *via* aminothiazole passivation†

Zewei Zhu,‡[ab] Bingcan Ke,‡[ab] Kexuan Sun,‡[c] Chengkai Jin,[a] Zhenhua Song,[c] Ruixuan Jiang,[a] Jing Li,[a] Song Kong,[a] Chang Liu,*[c] Sai Bai,[d] Sisi He,[e] Ziyi Ge,[c] Fuzhi Huang,*[ab] Yi-Bing Cheng[ab] and Tongle Bu*[a]

The passivation of undesirable defects in the perovskite light-absorption layer is an essential and effective strategy for improving the performance of perovskite solar cells (PSCs). Herein, a novel additive, 5-aminothiazole hydrochloride (5ATCl), possessing both electron-accepting (NH_3^+) and electron-donating (C═N) functional groups, is introduced into the perovskite precursor ink, enabling holistic improvements of perovskite thin-film quality and photovoltaic performance. Comprehensive theoretical calculations and experimental characterizations reveal strong hydrogen bonds and intermolecular coordination between 5ATCl with the perovskite components. Consequently, the perovskite films demonstrate increased grain size and improved film quality, along with a released residual stress and a reduced defect density. Furthermore, the 5ATCl contributes to a favorable energy level alignment, thus promoting charge transfer and minimizing open-circuit voltage loss of the resulting devices. Notably, the champion power conversion efficiencies (PCEs) of the rigid and flexible PSCs with the incorporation of 5ATCl reach 26.38% (certified 25.87%) and 24.54%, respectively. The stability of the devices is also enhanced, demonstrating a T_{90} lifetime of 850 hours under continuous light illumination at maximum power point tracking. Additionally, centimeter-sized PSCs and 5 cm × 5 cm solar mini-modules also demonstrate impressive PCEs of 24.86% and 21.72% respectively, indicating the great feasibility of our strategy in up-scaling device fabrication.

Received 24th February 2025,
Accepted 21st March 2025

DOI: 10.1039/d5ee01083g

rsc.li/ees

Broader context

The rapid development of perovskite solar cells (PSCs) has positioned them as one of the most promising technologies for next-generation photovoltaics, offering a compelling combination of high efficiency, low fabrication costs, and compatibility with flexible substrates. However, several challenges remain to bridge the performance gap between laboratory-scale devices and large-area industrial modules. One of the key challenges is the presence of undesirable defects in perovskite layers, which significantly impairs device efficiency and operational stability. Although numerous defect passivation strategies have been widely explored, many of them suffer from limited flexible scalability, incomplete defect mitigation, or incompatibility with large-area processing. In this study, we introduce a multifunctional additive, 5-aminothiazole hydrochloride (5ATCl), which simultaneously passivates ionic and coordinative defects *via* hydrogen bonding and molecular interactions, respectively. This multidimensional passivation strategy significantly improves the quality and optoelectronic properties of perovskite films. Our findings demonstrate significant enhancements in efficiency (26.38% for rigid devices), mechanical flexibility (24.54% for flexible PSCs), and operational stability ($T_{90} > 850$ h). Additionally, the successful fabrication of centimeter-scale devices (24.86%) and mini-modules (21.72%) underscores the effectiveness and practical applicability of this strategy.

---

[a] *State Key Laboratory of Advanced Technology for Materials Synthesis and Processing, Wuhan University of Technology, Wuhan 430070, P. R. China. E-mail: tongle.bu@whut.edu.cn, fuzhi.huang@whut.edu.cn*
[b] *Xianhu Laboratory of the Advanced Energy Science and Technology Guangdong Laboratory, Foshan 528200, P. R. China*
[c] *Zhejiang Provincial Engineering Research Center of Energy Optoelectronic Materials and Devices, Ningbo Institute of Materials Technology & Engineering, Chinese Academy of Sciences, Ningbo 315201, P. R. China. E-mail: liuchang1@nimte.ac.cn*
[d] *Institute of Fundamental and Frontier Sciences, University of Electronic Science and Technology of China, Chengdu 611731, P. R. China*
[e] *School of Science, Harbin Institute of Technology (Shenzhen), Shenzhen 518055, P. R. China*

† Electronic supplementary information (ESI) available. See DOI: https://doi.org/10.1039/d5ee01083g

‡ These authors contributed equally to this work.

1. Introduction

Organic–inorganic hybrid metal halide perovskite solar cells (PSCs) have attracted great attention due to their outstanding photovoltaic properties and great potential for commercial deployment.[1–3] Although the certified power conversion efficiency (PCE) for lab-scale single-junction PSCs has surged from 3.8% to 27%, it remains far below the Shockley–Queisser (S–Q) limit, especially that of large-scale solar modules.[4–8] The undesirable non-radiative recombination losses associated with defects at the interfaces and grain boundaries are undoubtedly a key causation that should be carefully addressed.[9,10] Therefore, the development of an effective passivation strategy is essential for pursuing high-quality perovskite films with inherently low defect densities, thus contributing to efficient and stable PSCs and solar modules.

Previous studies have shown that high-density defects at the grain boundaries and interfaces significantly influence nonradiative recombination,[11] which affects carrier transport and ion migration sequentially. Considerable defect passivation methods have been developed in recent years to improve the performance of PSCs.[12] These methods typically involve the passivation of positive Pb^{2+} defects and negative halide defects to reduce nonradiative recombination losses.[13,14] Generally, passivation materials containing multifunctional groups, such as halides or pseudo halides (such as Cl, SCN, BF_4, PF_6, *etc.*)[15–18] and small molecules (such as theophylline, 2-aminoterephthalic acid, phenylethylamine, *tert*-butylbenzylammonium, and naphthylmethylamine, *etc.*),[19–22] are widely used due to their ability to simultaneously passivate both positively and negatively charged defects. In particular, functional groups containing elements like N, O, and S, which possess lone electron pairs, can serve as Lewis bases to effectively passivate positively charged defects.[19,23–27] Therefore, the rational design of materials with efficient passivation functional groups is essential.

The efficiency and stability of PSCs are predominantly governed by the effectiveness of defect passivation strategies, as well as the selection of passivation materials, which play a crucial role in mitigating defects within the perovskite films. Drawing from the literature, phenylethylammonium iodide (PEAI) has emerged as a prevalent passivation agent for both bulk and surface perovskite films, leveraging its amino group ($-NH_3^+$) to form coordination bonds with under-coordinated lead ions and passivate cation vacancies.[28,29] Recently, Tan *et al.* proposed a new passivation agent, 4-trifluoromethylphenylammonium (CF_3–PA), that exhibits a greater electropositivity on the $-NH_3^+$ side and shows a stronger interaction with perovskites than PEA, leading to improved perovskite crystallinity and device performance.[30] Qiu *et al.* first introduced a novel *in situ* polymerization strategy of the monomer containing $-CF_3$ groups inside the precursor, forming a polymer chain binding agent for the improved quality of the active layer.[31] Moreover, incorporating elements with lone pairs of electrons, such as S or N, into passivation agents can form strong interactions with the perovskite lattice, thereby enhancing passivation effects. For example, Yang *et al.* reported that thienylmethylamine (TMA) outperforms PEA in photovoltaic performance due to strong Pb–S interactions and electron-rich π-functional groups in the thienyl moiety, which effectively passivate Pb^{2+} defects and enhance charge mobility.[32] Kanatzidis *et al.* demonstrated that thiazole additives, featuring both S and N donor atoms, can enhance perovskite film quality by promoting high crystallinity, large grain sizes, and low roughness, while significantly reducing the defect density.[32] Qin *et al.* introduced imidazole derivatives, specifically 2-(aminomethyl) imidazole dihydrochloride (2-AD), into Sn–Pb mixed perovskites, demonstrating that the lone pair electron of N and the $-NH_2$ group can coordinate with metal ions to regulate the crystallization process and improve the homogeneity of the perovskite film.[33]

Inspired by the preceding work, herein, a novel multifunctional thiazole-based passivation agent, 5-aminothiazole hydrochloride (5ATCl), is introduced to modulate the quality of perovskite films. We propose that the electron-rich nitrogen (N) of the thiazole ring coupled with the $-NH_3^+$ group could strongly interact with the uncoordinated Pb^{2+}. Moreover, the electron-withdrawing $-NH_3^+$ group has the capability to form hydrogen bonds with FAI and coordination bonds with $[PbI_6]^{4-}$ octahedra, thus achieving a multi-site passivation effect for the perovskite films. As a result, the 5ATCl-passivated perovskite films exhibit significantly enhanced crystallinity with larger grains, uniform surface potential, and more ideal energy level alignment. Benefiting from the multifunctional passivation effect of 5ATCl, the 1.55 eV inverted PSCs achieved a champion PCE of 26.38% with an outstanding open-circuit voltage (V_{OC}) of 1.202 V and a high fill factor (FF) of 85.39%. The corresponding devices demonstrate a certified PCE of 25.87% and a stabilized certified efficiency of 25.53%, achieving the highest $V_{OC} \times FF$ value reported to date. Additionally, this passivation strategy not only enables the fabrication of high-efficiency small-sized flexible PSCs with a champion PCE of 24.54% but also demonstrates scalability for centimeter-sized rigid PSCs with an impressive PCE of 24.86% and 5 cm × 5 cm solar minimodule with a PCE of 21.72%. Moreover, this passivation strategy significantly enhances the device stability under thermal and light stresses, demonstrating a T_{90} lifetime of over 850 hours under continuous light illumination at maximum power point (MPP) tracking. This study provides valuable insights into the synergistic passivation mechanism of aminothiazole and would be insightful for advanced designs of aminothiazole derivatives in the photovoltaic field.

2. Results and discussion

2.1. Interactions between 5ATCl and perovskite

The electrostatic potential distribution of the 5ATCl molecule is calculated and depicted in Fig. S1 (ESI†). The maximum electrostatic potential (ESP) near the NH_3^+ group enhances the binding strength between the ligand and the surface cation vacancy site of the perovskite, such as FA or MA vacancies (V_{MA} or V_{FA}), and Pb vacancies (V_{Pb}). Furthermore, the $-NH_3^+$

group can form coordination bonds with under-coordinated lead ions,[34] and the negatively charged N and S elements in the thiazole can passivate positively charged defects, such as I vacancies (V_I) and (Pb_I), thereby reducing the defect density of the perovskite films. To further elucidate the interaction between 5ATCl and perovskites, density functional theory (DFT) calculations were conducted to investigate the adsorption state and electronic structure of 5ATCl on α-$FAPbI_3$ perovskite surfaces (Fig. 1a, b and Fig. S2a–f, ESI†). The formation energies of various defects on PbI_2-terminated and FAI-terminated perovskite surfaces with and without the adsorption of 5ATCl are shown in Fig. 1c. For the PbI_2 termination, the $-NH_3^+$ functional group exhibits strong charge transfer with PbI termination indicating a strong interaction between them, resulting in the increased formation energies of V_I, V_{Pb}, Pb_I, I–Pb, and I_i. A similar phenomenon is also observed at the surface termination of FAI, in which the formation energy of V_{FA} also increased significantly after 5ATCl adsorption. These results suggested that the introduction of 5ATCl can interact with perovskites to inhibit defect formation and effectively reduce the defect density of perovskite films.

To explore the potential interactions between 5ATCl and perovskites, ^1H nuclear magnetic resonance (^1H-NMR) spectroscopy was performed on 5ATCl, pure FAI, PbI_2, and their mixtures (Fig. S3, ESI†). As illustrated in Fig. 1d, the peaks at 8.81 ppm and 7.86 ppm for pure FAI correspond to the $-NH_2$ and –CH groups of FAI, respectively. When FAI is mixed with 5ATCl, the $-NH_2$ peak of FAI splits into three peaks at 9.04 ppm, 8.77 ppm, and 8.74 ppm, while the NH_3^+ peak of 5ATCl shifts from 9.25 ppm to 9.15 ppm. This observed shift indicates an interaction between 5ATCl and ammonium/hydrogen-bonded carbon atoms. Moreover, the –CH peak of FAI splits to a triplet

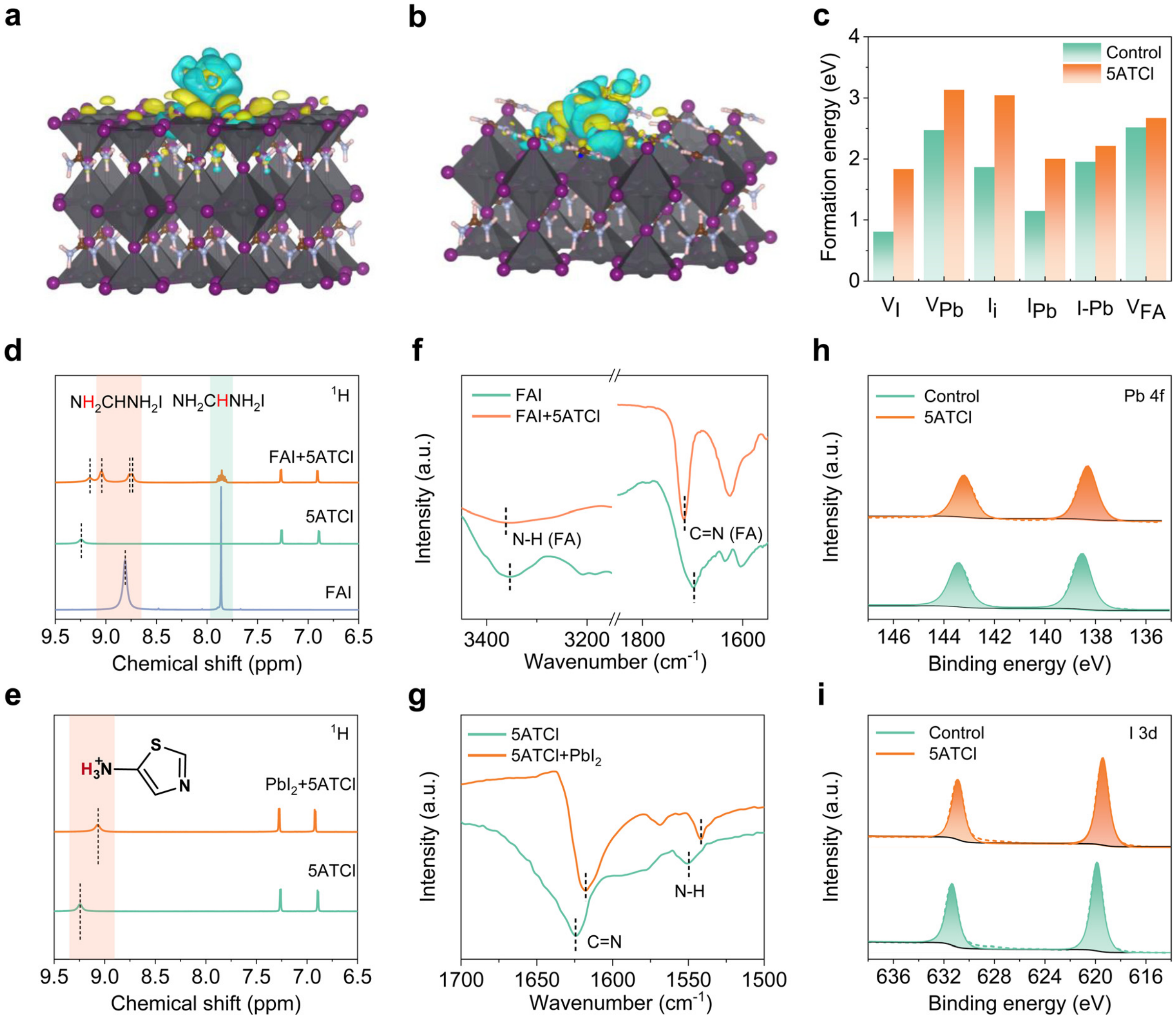

Fig. 1 Interactions between 5ATCl and perovskite. Electron-density distribution after adsorption of 5ATCl on different $FAPbI_3$ surfaces, (a) PbI_2-terminated surface and (b) FAI-terminated surface. The yellow regions represent areas of increased charge, and the light blue regions represent areas of decreased charge. (c) Formation energies of surface Pb and I vacancy defects, Pb and I substitution defects, interstitial defects, and FA vacancy defects adsorbed on the control and 5ATCl-modified samples. Liquid-state ^1H-NMR spectra of (d) FAI, 5ATCl, and FAI mixed with 5ATCl. (e) 5ATCl and PbI_2 mixed with 5ATCl, (f) FTIR spectra enlarged N–H, and C═N stretching peaks of FAI and FAI mixed with 5ATCl, and (g) 5ATCl and 5ATCl mixed with PbI_2. XPS spectra of (h) Pb 4f and (i) I 3d of different perovskite films.

of triplets due to coupling with the two different amidine protons,[23] suggesting changes in the surrounding hydrogen chemical environment, thereby confirming the formation of hydrogen bonds between FAI and 5ATCl.[35,36] Similarly, an obvious chemical shift in the $-NH_3^+$ peak is evident when 5ATCl is mixed with PbI_2 (Fig. 1e), indicating a strong interaction between 5ATCl and PbI_2. Fourier-transform infrared spectroscopy (FTIR) analyses were performed to further elucidate the chemical interactions between 5ATCl and the perovskite components, as shown in Fig. 1f and g, and Fig. S4a and b (ESI†). Upon mixing 5ATCl with FAI, the N–H stretching peak of FA^+ shifted from 3353 cm^{-1} to 3355 cm^{-1}, and the C=N stretching peak of FA^+ shifted from 1698 cm^{-1} to 1717 cm^{-1}, indicating the formation of hydrogen bonds between 5ATCl and FAI.[37] Similarly, in the mixture of 5ATCl and PbI_2, the N–H stretching peak of 5ATCl shifted from 1550 cm^{-1} to 1541 cm^{-1}, and the C=N stretching peak of 5ATCl shifted from 1624 cm^{-1} to 1618 cm^{-1}. These shifts provide evidence of interactions between 5ATCl and PbI_2, specifically the formation of N–H···Pb and C=N···Pb interactions.[38–40]

To further elucidate the chemical state changes between 5ATCl and perovskite, X-ray photoelectron spectroscopy (XPS) characterization of the perovskite films was performed. As shown in Fig. 1h and i, obvious shifts in the Pb 4f and the I 3d signals were observed upon the addition of 5ATCl, indicating the formation of coordination bonds between 5ATCl and the perovskites.[41] Specifically, the shift of the I 3d signals to lower binding energies suggests strong coordination between the $-NH_3^+$ groups of 5ATCl and I^- leading to an increase in the electron cloud density, indicative of suppressed V_I defects around the perovskite grain boundaries.[42,43] Moreover, Fig. S5b (ESI†) illustrates that the N 1s signal shifted from 400.6 eV to 400.3 eV after 5ATCl incorporation, evidencing the formation of hydrogen bonds between the nitrogen atoms in 5ATCl and the perovskite. We speculate that the strong chemical interactions induced by the 5ATCl molecule would enhance the electronic structure of the perovskite film, thereby potentially passivating the defects within the perovskites.

2.2. Effects of 5ATCl on perovskite morphology and crystallinity

To investigate the effect of 5ATCl addition on the crystallinity of the perovskite, scanning electron microscopy (SEM) and atomic force microscopy (AFM) were performed to observe changes in the perovskite morphologies. Fig. 2a–c and Fig. S6 (ESI†) illustrate a significant increase in grain size and an obvious reduction in grain boundaries of perovskite films upon the incorporation of an appropriate concentration of 5ATCl. Fig. S7c and d (ESI†) demonstrate a reduction in the root mean square (RMS) of the surface roughness from 12.4 nm to 8.6 nm after the addition of 5ATCl, indicating a smoother interface with the adjacent electron transfer layer. Besides, grazing incident wide-angle X-ray scattering (GIWAXS) and X-ray diffraction (XRD) were further performed as shown in Fig. S8a–d (ESI†). It clearly shows the dramatically enhanced intensity of the (001) peak either from the surface or bulk, which is favorable in the formation of high-quality films with a lower defect density.

The depth-resolved grazing incidence X-ray diffraction (GIXRD) measurements were further conducted to investigate the effect of 5ATCl on the residual strain of the perovskite films. As shown in Fig. 2d and e, with the incident angle increasing from 0.2 to 1.0 $Å^{-1}$, the (001) diffraction peak of the control film shifts to lower angles along the q-axis, indicating residual tensile stress within the perovskite film. As a comparison, the (001) diffraction peak of the 5ATCl-incorporated film shows minimal shift as the incident angle increases, confirming the reduction in residual stress. After adding 5ATCl, the slope of the fitted line decreased from 3.57×10^{-4} to 2.33×10^{-4} (Fig. 2f), indicating the release of residual strain in the perovskite film. Such an outcome is likely attributed to the coordination and hydrogen bonding interactions between 5ATCl and the perovskite, which could stabilize the octahedral lattice, thereby reducing the trap density in the modified perovskite films.[44–46]

Subsequently, the energy levels of perovskite films with and without 5ATCl were measured using ultraviolet photoelectron spectroscopy (UPS). The corresponding UPS spectra and energy level diagrams are shown in Fig. 2g and Fig. S9a–f (ESI†). The valence band maximum (VBM) and conduction band minimum (CBM) of the perovskite films were determined, with the cutoff region (E_{cutoff}) used for this analysis. After incorporating 5ATCl, the Fermi level (E_F) shifted from −5.09 eV to −5.19 eV, as shown in Fig. 2h, which is consistent with the KPFM results (Fig. S10, ESI†). Additionally, the energy difference between the Fermi level and the conduction band (CBM) for the 5ATCl-modified perovskite film was 0.81 eV, which is lower than that of the control perovskite film (0.84 eV). This suggests that the 5ATCl-modified perovskite film exhibits more pronounced n-type characteristics.[47] In addition, the specific energy level alignment between the C_{60} layer and perovskite films before and after 5ATCl modification is illustrated in Fig. 2i. In comparison to the control films (Δ = 0.50 eV), the 5ATCl-modified films (Δ = 0.60 eV) exhibit a larger Fermi level difference (Δ) with C_{60},[48,49] indicating a stronger additional built-in electric field at the perovskite/C_{60} interface. This is expected to result in more efficient charge transport and collection, leading to facilitated charge extraction and an improvement in the V_{OC}.

2.3. Passivation of perovskite defects

To evaluate the passivation effects of 5ATCl on the perovskite films, photoelectric characterizations were systematically performed. Fig. 3a and b show the femtosecond transient absorption spectroscopy (TAS) results for perovskite films with and without the addition of 5ATCl. The TAS pseudocolor maps for both types of perovskite films exhibit strong negative ground-state photobleaching (PB) peaks at ∼800 nm, which are associated with the filling of the conduction band edge. Significantly, the intensity of the PB peak was substantially enhanced in the 5ATCl-modified perovskite film compared to the control, suggesting an increase in the number of photoexcited excitons. The exciton decay dynamics, obtained by fitting the decay curves with a bi-exponential function, reveal that the decay

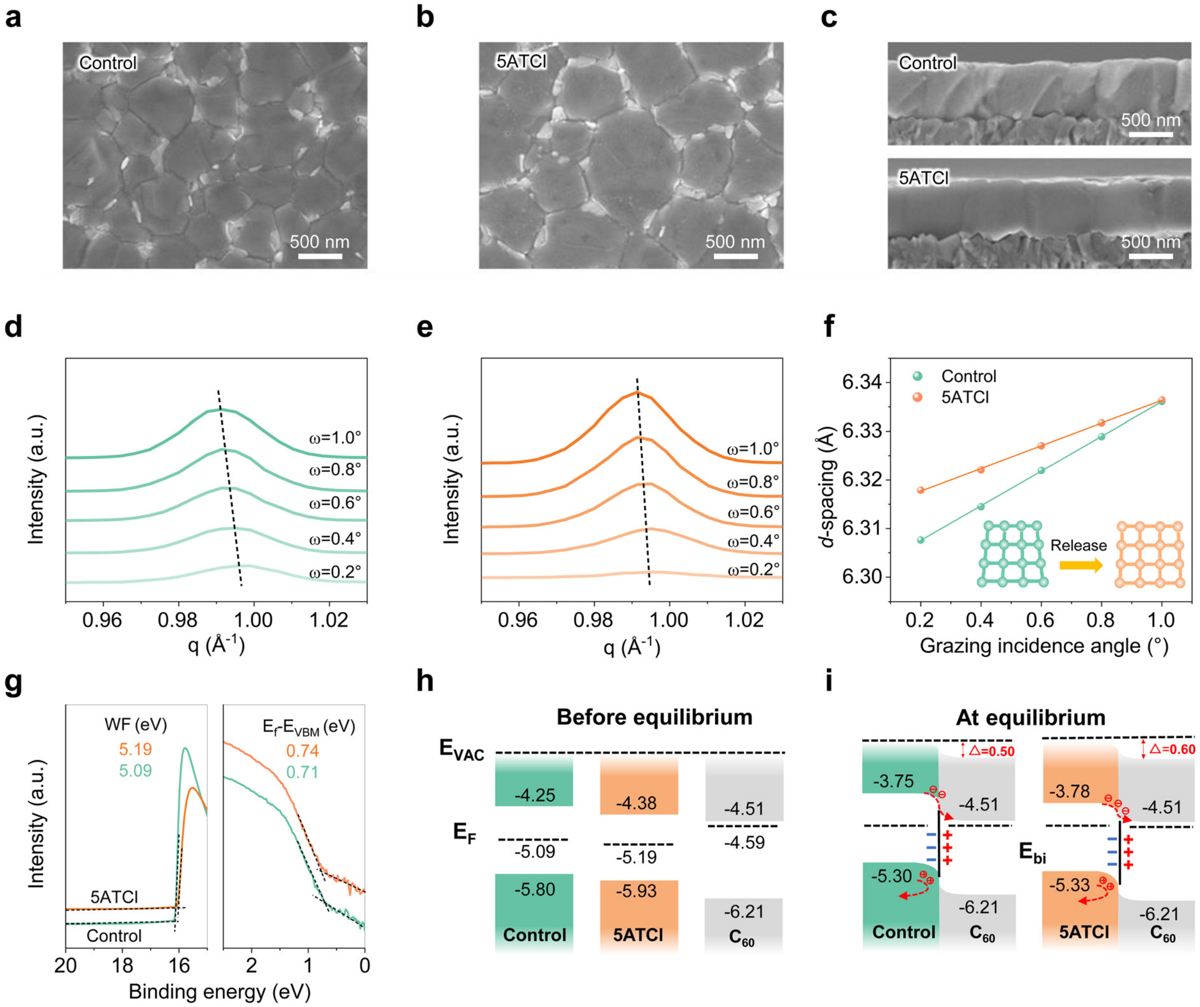

Fig. 2 Surface structures and energy level alignments of the control and 5ATCl-modified perovskite films. Top-view SEM images of the (a) control and (b) 5ATCl-modified perovskite films. Cross-sectional SEM images of the (c) control and 5ATCl-modified perovskite films. GIXRD spectra of the (d) control and (e) 5ATCl-modified perovskite films. (f) Linear fit of *d*-spacing *versus* grazing incidence angle curves of the control and 5ATCl-modified perovskite films. (g) UPS spectra of the control and 5ATCl-modified perovskite films. (h) Individual measurements of energy levels of the control and 5ATCl-modified perovskite films, and (i) the corresponding band-bending schematics. E_{vac}, vacuum level; E_F, Fermi level, built-in electric field at the junction.

lifetime of the 5ATCl-modified perovskite film is 502.77 ps, much higher than that of the control film, which is 126.13 ps (Fig. 3c and Table S1, ESI†). This indicates that the reduction of defect states and non-radiative recombination may contribute to the extension of the decay lifetime.[50] Additionally, the photophysical process of the modified film was observed to be slower than that of the control sample (Fig. 3d and e), suggesting a weaker bandgap oscillation and indicating suppression of the background carrier density due to a reduced defect density.

Following this, steady-state and time-resolved photoluminescence (TRPL) measurements were performed using structures of glass/perovskite and glass/perovskite/C_{60}, respectively. When the excitation light was incident on the surface of the perovskite films, the emission intensity of the 5ATCl-modified film at around 800 nm was significantly higher than that of the control film (Fig. 3g). The TRPL data also indicated that the carrier lifetime in the 5ATCl-modified film was correspondingly increased (Fig. 3h and Table S2, ESI†), indicating suppressed non-radiative recombination and thereby enhanced photovoltaic performance of the perovskite film.[51] Meanwhile, when the excitation light is from the C_{60} side, the 5ATCl-modified perovskite films exhibit a lower PL intensity and a shorter PL lifetime (Fig. S11 and Table S3, ESI†), indicating accelerated interface charge transfer and thereby enhanced device photovoltaic performance due to the passivation effect of 5ATCl.[52] Furthermore, the PL quantum yield (PLQY) of the 5ATCl-modified perovskite film (9.50%) was more than twice that of the control film (3.85%), with a corresponding increase in quasi-Fermi level splitting (QFLS) by 24 mV (Fig. 3f), which is calculated referring to previous reports.[53] We further performed space charge limited current (SCLC) measurements to quantitatively evaluate the trap density.[54] As shown in Fig. 3i, the defect concentration of the perovskite film decreased significantly from 1.08×10^{15} cm^{-3} to 0.90×10^{15} cm^{-3} after 5ATCl incorporation. These results indicate that the quality of the perovskite films was improved and non-radiative

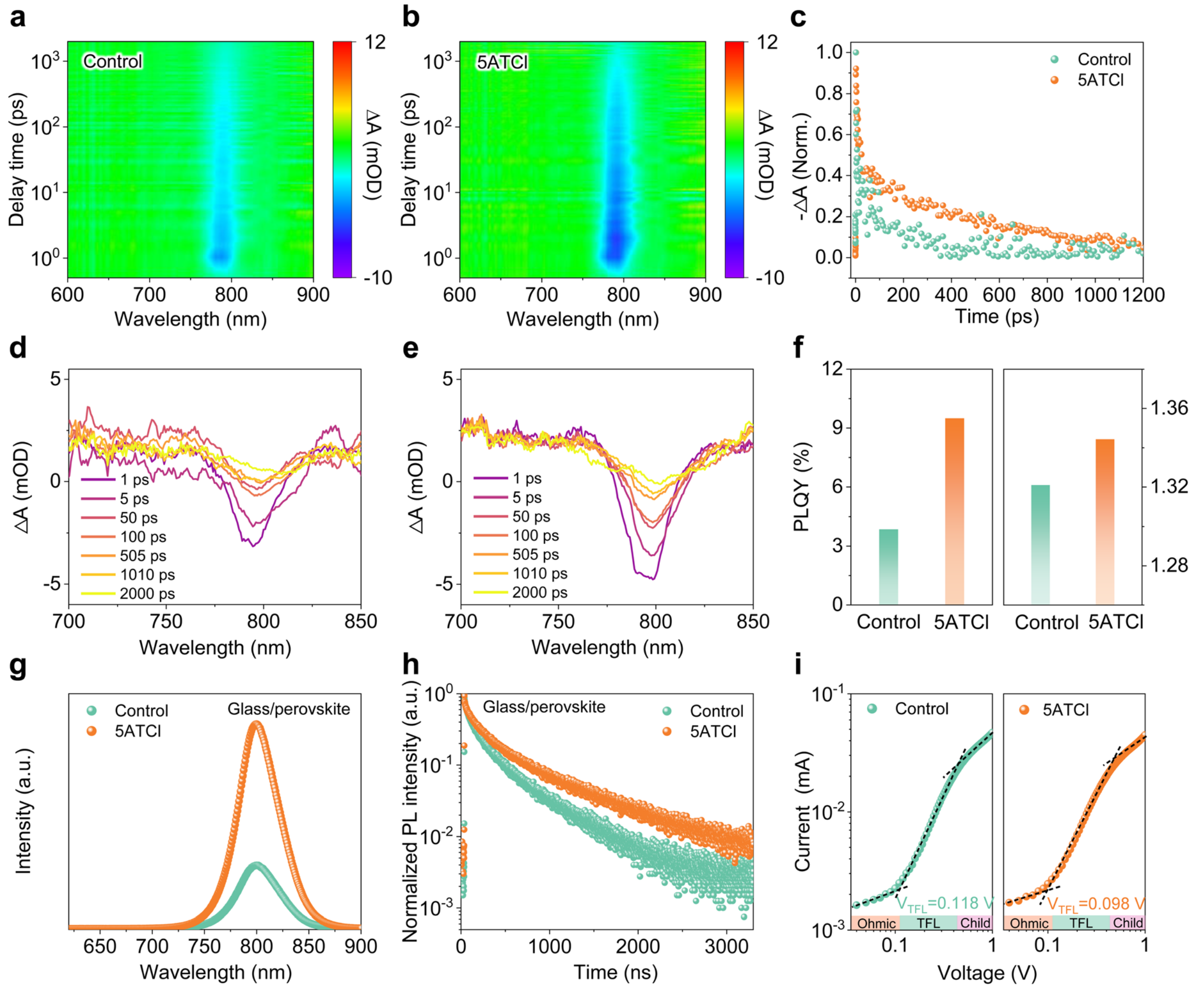

Fig. 3 Properties of perovskite films. The pseudo-color TA plots of the (a) control and (b) 5ATCl-modified perovskite films. (c) The normalized kinetic traces for photo-bleaching probed at 798 nm of the control and 5ATCl-modified perovskite films. TA spectra at different delay times of the (d) control and (e) 5ATCl-modified perovskite films under front excitation. (f) PLQY of different perovskite films deposited on the glass substrates. (g) Steady-state PL spectra and (h) TRPL results of the control and 5ATCl-modified perovskite films. (i) SCLC test of the control and 5ATCl-modified perovskite films.

recombination losses were reduced due to the effective passivation effect of 5ATCl.

2.4. Characterization of photovoltaic performance

To evaluate the photovoltaic performance of PSCs modified with 5ATCl, an inverted device with the structure of glass/FTO/Ph-4PACz/perovskite/C_{60}/BCP/Ag was fabricated as depicted in Fig. 4a. The *J*–*V* curves of the champion PSCs, both with and without the introduction of 5ATCl, are shown in Fig. 4b. Notably, the 5ATCl-modified PSC demonstrated an impressive PCE of 26.38%, along with a significantly enhanced V_{OC} of 1.202 V and an increased FF of 85.39%, significantly higher than that of the control devices. An analysis of the device statistics for both the control and 5ATCl-modified PSCs revealed a significant enhancement in PCE, primarily due to the increase in V_{OC} and FF, as shown in Fig. S12–S13 and Table S4 (ESI†). This improvement in V_{OC} and FF for the 5ATCl-modified device can be ascribed to the reduction in charge recombination and the optimization of energy band alignment, as discussed previously. The corresponding stable power output (SPO) was 26.36% for the 5ATCl-modified and 25.43% for the control devices, respectively, closely aligning with the PCE derived from *J*–*V* measurements (Fig. 4c). The integrated photocurrent densities from the external quantum efficiency (EQE) spectrum (25.48 mA cm^{-2}) are well-matched with the J_{SC} in Fig. S14 and S15 (ESI†). The device performance was also validated by a third party, the National PV Industry Measurement and Testing Center. It demonstrated certified PCEs of 25.87% under reverse scan and 25.65% under forward scan, respectively, and delivered a certified stabilized efficiency of 25.53% (Fig. S16, ESI†). Furthermore, this passivation strategy was also successfully applied to flexible PSCs, which achieved a significantly enhanced PCE of 24.54%, and the corresponding SPO was 24.45% (Fig. 4d, e, Fig. S17, and Table S5, ESI†). Notably, as highlighted in Fig. 4f, the V_{OC} × FF values of the rigid and flexible PSCs reached 1.027 and 1.001, respectively,

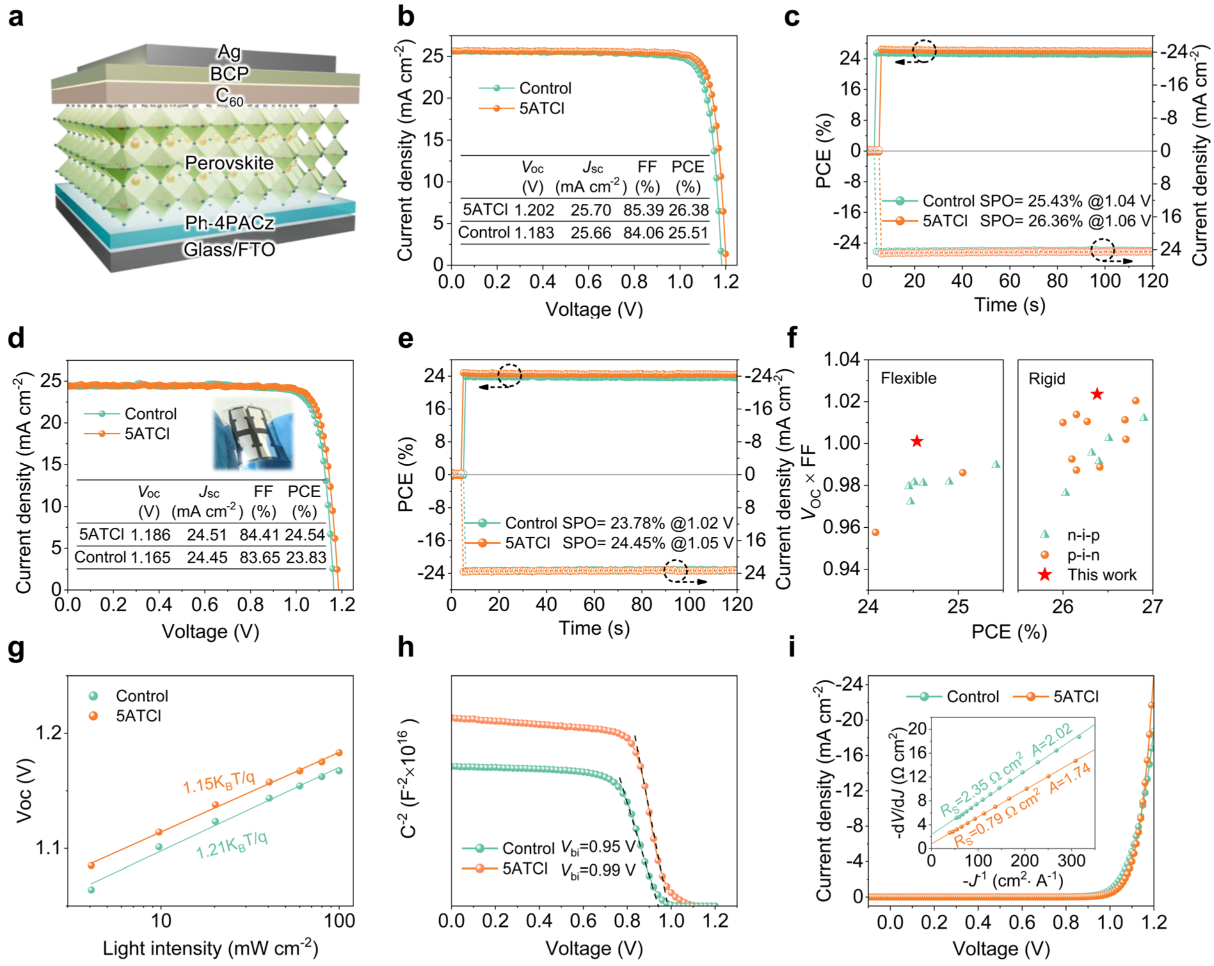

	V_{oc} (V)	J_{sc} (mA cm^{-2})	FF (%)	PCE (%)
5ATCl	1.202	25.70	85.39	26.38
Control	1.183	25.66	84.06	25.51

	V_{oc} (V)	J_{sc} (mA cm^{-2})	FF (%)	PCE (%)
5ATCl	1.186	24.51	84.41	24.54
Control	1.165	24.45	83.65	23.83

Fig. 4 Photovoltaic performances of the PSCs with and without 5ATCl modification. (a) Schematic diagram of the device structure. (b) *J–V* curves and (c) the corresponding steady-state power output of the champion rigid devices. (d) *J–V* curves and (e) the corresponding steady-state power output of the champion flexible devices. (f) Comparison of the PCEs and $V_{OC} \times$ FF values of high-efficiency flexible and rigid PSCs reported in the literature (listed in Tables S6 and S7, ESI†). (g) V_{OC} *versus* light intensity plots, (h) Mott–Schottky curves, and (i) dark *J–V* curves of the typical rigid devices with and without 5ATCl modification. The inset shows the corresponding linear relationship of $-\mathrm{d}V/\mathrm{d}J$ and $-J^{-1}$.

which are among the highest values reported recently (Tables S5 and S6, ESI†).

In addition, the linear relationship between V_{OC} and light intensity is depicted in Fig. 4g. Through linear fitting, the ideal factor for the 5ATCl-modified devices was determined to be $1.15k_BT/q$, much lower than that of the $1.21k_BT/q$ of the control devices, indicating that 5ATCl plays a crucial role in suppressing non-radiative recombination. The Mott–Schottky results in Fig. 4h reveal an increased built-in voltage (V_{bi}) of the PSCs from 0.95 V to 0.99 V following 5ATCl passivation, explaining the enhanced V_{OC} in these devices. Fig. 4i shows the *J–V* curves under dark conditions and the corresponding determined series resistance (R_S) and ideal factor (A) were calculated according to previous reports.[55,56] Analysis of the linear fitting data for the slope and intercept revealed that R_S of the 5ATCl-modified devices decreased from 2.35 Ω cm^2 to 0.79 Ω cm^2, while the A dropped from 2.02 to 1.74. These changes suggest a reduction in non-radiative recombination losses and a decrease in defect density, contributing to improved device performance.[57]

2.5. Stability and scalability of solar cells

The passivation effect of 5ATCl on the stability of PSCs was evaluated by characterizing devices under various conditions. As shown in Fig. 5a, the 5ATCl-modified devices maintained 87.9% of their initial PCE under continuous heating at 65 °C in an N_2 environment for 700 h. In contrast, the control devices only maintain 73.9% of their initial PCE, thereby indicating a significant enhancement in thermal stability upon 5ATCl modification. This improvement can be attributed to the effective mitigation of residual strain in the films upon 5ATCl modification. Moreover, under continuous 1-sun illumination in ambient air with a controlled temperature of approximately 25 °C, the 5ATCl-modified PSCs demonstrated a T_{90} lifetime of ~850 hours at MPP tracking, which is significantly superior to that of the control devices. The corresponding *J–V* curves before and after the MPP tracking test are available in Fig. S18 (ESI†). These results demonstrate that the 5ATCl-modified devices exhibit excellent thermal and operational stability.

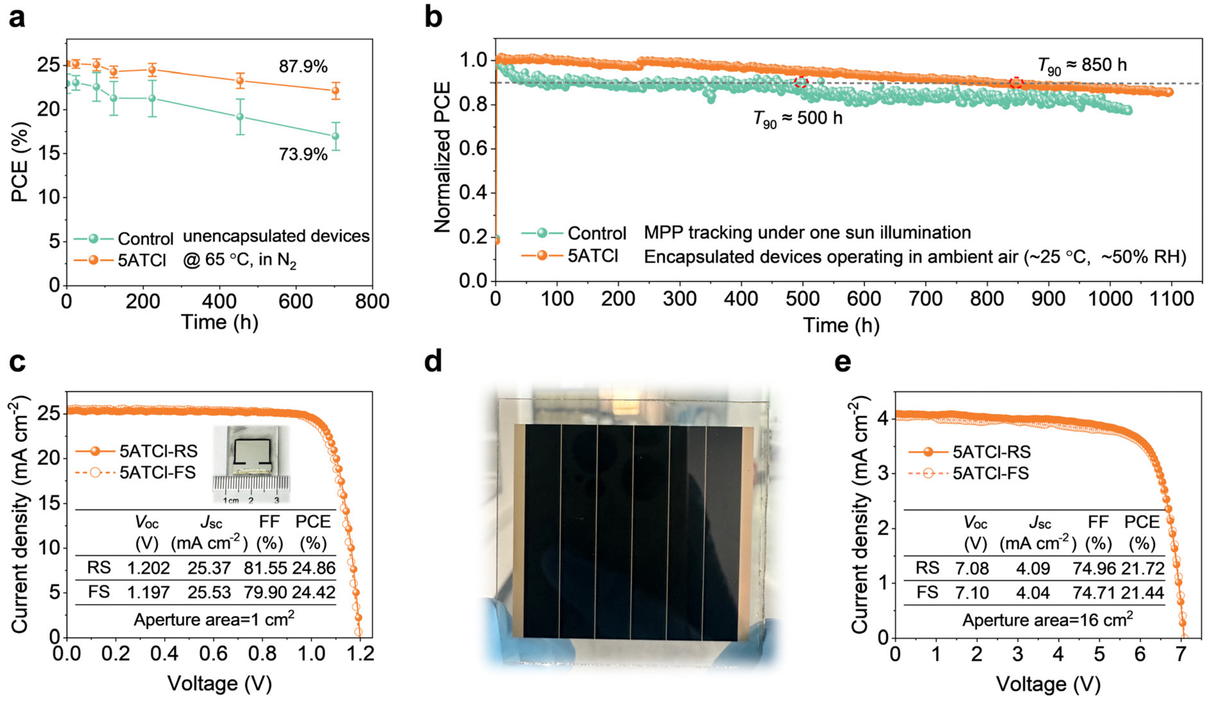

Fig. 5 Stability and scalability of PSCs. (a) Thermal stability of the unencapsulated PSCs with and without 5ATCl modification. (b) Operating stability of the encapsulated PSCs with and without 5ATCl modification. (c) *J–V* curves of the champion large-size PSCs with 5ATCl modification, with the inset showing the device picture. (d) The photograph and (e) *J–V* curve of the champion 5 cm × 5 cm mini-module with 5ATCl modification.

To further explore the feasibility of 5ATCl modification in upscaling fabrication, large-sized (1 cm^2) solar cells and 5 cm × 5 cm solar mini-modules were fabricated. As shown in Fig. 5c, the 1 cm^2 PSCs achieved a PCE of 24.86%, with a high V_{OC} of 1.202 V, a J_{SC} of 25.37 mA cm^{-2}, and an FF of 81.55%, delivering an SPO of 24.66% (Fig. S19, ESI†). Notably, the $V_{OC} \times J_{SC}$ values of the large-area devices were comparable to those of small-area devices, indicating the great viability for upscaling. Additionally, the 5 cm × 5 cm solar mini-module with a high geometric fill factor (GFF) of 0.96 is demonstrated as shown in Fig. 5d and Fig. S20 (ESI†). Fig. 5e shows the *J–V* curve, in which a commendable PCE of 21.72% is demonstrated. These results confirm that 5ATCl passivation remains effective in preserving efficiency during upscaling, highlighting its potential for future commercial applications.

3. Conclusion

In summary, the passivation mechanism of perovskite films utilizing a multifunctional additive 5ATCl was systematically investigated. A comprehensive combination of experimental and theoretical calculations demonstrates that the 5ATCl molecule can form hydrogen bonds and coordinate with perovskites, resulting in strong interactions with interface defects. Experimental analyses reveal that perovskite films passivated with 5ATCl displayed a reduced defect density, suppressed non-radiative recombination, improved energy level alignment, and hindered hole transport across the interface between the perovskite and electron transport layers. Consequently, leveraging the superior defect passivation ability of 5ATCl, impressive PCEs of 26.38% with a high V_{OC} of 1.202 V for rigid devices and 24.54% for flexible devices were achieved, along with excellent thermal and operational stability. Notably, the V_{OC} × FF values for both the rigid and flexible PSCs achieve the highest values among recent reports. Furthermore, applying this strategy in scaled-up manufacturing yielded impressive PCEs of 24.86% for a centimeter-sized solar cell and 21.72% for a 5 cm × 5 cm solar mini-module, respectively. The utilization of 5ATCl as a passivator presents considerable promise for the development of high-performance PSCs.

Author contributions

T. B., F. H., and C. L. supervised this work. T. B. and Z. Z. conceived the ideas and designed the experiments. Z. Z. and B. K. prepared the samples and devices and performed the corresponding basic characterization. K. S. conducted the DFT calculation and analysis. C. J. and S. K. helped with the module fabrication. R. J., J. L., S. B., S. H., Z. G. and Y.-B. C. provided valuable suggestions for the manuscript. T. B. and Z. Z. participated in all the data analysis and finished this paper, and all authors reviewed the paper.

Data availability

The data that support the findings of this study are available from the corresponding author upon reasonable request.

Conflicts of interest

The authors declare no competing interests or conflicts.

Acknowledgements

This work was supported by funding from the National Natural Science Foundation of China (52202292, 22279099, 52322315, and 52172230), the Guangdong Pearl River Talent Program (2021ZT09L400), the Fundamental Research Funds for the Central Universities (WUT: 2023IVB074, 2023IVB077, 2023IVB008), the State Key Laboratory of Advanced Technology for Materials Synthesis and Processing (Wuhan University of Technology: 2024-KF-10), and the Chengdu Science and Technology Program (2024-JB00-00010-GX).

References

1 Q. Jiang and K. Zhu, *Nat. Rev. Mater.*, 2024, **9**, 399–419.
2 J. Y. Kim, J.-W. Lee, H. S. Jung, H. Shin and N.-G. Park, *Chem. Rev.*, 2020, **120**, 7867–7918.
3 J.-W. Lee, D.-J. Seol, A.-N. Cho and N.-G. Park, *Adv. Mater.*, 2014, **26**, 4991–4998.
4 A. Kojima, K. Teshima, Y. Shirai and T. Miyasaka, *J. Am. Chem. Soc.*, 2009, **131**, 6050–6051.
5 H.-S. Kim, C.-R. Lee, J.-H. Im, K.-B. Lee, T. Moehl, A. Marchioro, S.-J. Moon, R. Humphry-Baker, J.-H. Yum, J. E. Moser, M. Grätzel and N.-G. Park, *Sci. Rep.*, 2012, **2**, 591.
6 Z. Huang, Y. Bai, X. Huang, J. Li, Y. Wu, Y. Chen, K. Li, X. Niu, N. Li, G. Liu, Y. Zhang, H. Zai, Q. Chen, T. Lei, L. Wang and H. Zhou, *Nature*, 2023, **623**, 531–537.
7 J. Zheng, Z. Ying, Z. Yang, Z. Lin, H. Wei, L. Chen, X. Yang, Y. Zeng, X. Li and J. Ye, *Nat. Energy*, 2023, **8**, 1250–1261.
8 Y. Yang, R. Chen, J. Wu, Z. Dai, C. Luo, Z. Fang, S. Wan, L. Chao, Z. Liu and H. Wang, *Angew. Chem., Int. Ed.*, 2024, **63**, e202409689.
9 A. Rajagopal, K. Yao and A. K. Y. Jen, *Adv. Mater.*, 2018, **30**, 1800455.
10 Z. Dai, Y. Yang, X. Huang, S. Wan, L. Yuan, H. Wei, S. Nie, Z. Liu, Y. Wu, R. Chen and H. Wang, *Nano Energy*, 2024, **131**, 110190.
11 J. Zhang, S. Tang, M. Zhu, Z. Li, Z. Cheng, S. Xiang and Z. Zhang, *Energy Environ. Mater.*, 2024, **7**, 12696.
12 F. Gao, Y. Zhao, X. Zhang and J. You, *Adv. Energy Mater.*, 2019, **2020**, 1902650.
13 W. Jiarong, B. Leyu, H. Xiaofeng, F. Qifan, L. Ming, C. Mingqian, A. Yidan, J. Wenlin, R. L. Francis, F. Qiang and K. Y. J. Alex, *eScience*, 2024, **4**, 100308.
14 H. Chen, C. Liu, J. Xu, A. Maxwell, W. Zhou, Y. Yang, Q. Zhou, A. S. R. Bati, H. Wan, Z. Wang, L. Zeng, J. Wang, P. Serles, Y. Liu, S. Teale, Y. Liu, M. I. Saidaminov, M. Li, N. Rolston, S. Hoogland, T. Filleter, M. G. Kanatzidis, B. Chen, Z. Ning and E. H. Sargent, *Science*, 2024, **384**, 189–193.
15 J. Li, C. Jin, R. Jiang, J. Su, T. Tian, C. Yin, J. Meng, Z. Kou, S. Bai, P. Müller-Buschbaum, F. Huang, L. Mai, Y.-B. Cheng and T. Bu, *Nat. Energy*, 2024, **9**, 1540–1550.
16 W. Zhenhan, H. Zhaoyang, C. Xinbo, Z. Haitao, Y. Shiqi, Z. Qian, X. Zhuang, Q. Zihan, T. Hongbo, W. Wei, W. Fang, Y. Yongbo, L. Yun, Y. Yingguo, Z. Xingwang, J. Qi and Y. Jingbi, *Adv. Mater.*, 2024, **36**, 2407681.
17 S. Bai, P. Da, C. Li, Z. Wang, Z. Yuan, F. Fu, M. Kawecki, X. Liu, N. Sakai, J. T.-W. Wang, S. Huettner, S. Buecheler, M. Fahlman, F. Gao and H. J. Snaith, *Nature*, 2019, **571**, 245–250.
18 T. Bu, J. Li, H. Li, C. Tian, J. Su, G. Tong, L. K. Ono, C. Wang, Z. Lin, N. Chai, X.-L. Zhang, J. Chang, J. Lu, J. Zhong, W. Huang, Y. Qi, Y.-B. Cheng and F. Huang, *Science*, 2021, **372**, 1327–1332.
19 R. Wang, J. Xue, K.-L. Wang, Z.-K. Wang, Y. Luo, D. Fenning, G. Xu, S. Nuryyeva, T. Huang, Y. Zhao, J. L. Yang, J. Zhu, M. Wang, S. Tan, I. Yavuz, K. N. Houk and Y. Yang, *Science*, 2019, **366**, 1509–1513.
20 Z. Liu, F. Cao, M. Wang, M. Wang and L. Li, *Angew. Chem., Int. Ed.*, 2019, **59**, 4161–4167.
21 H. Zhu, Y. Liu, F. T. Eickemeyer, L. Pan, D. Ren, M. A. Ruiz-Preciado, B. Carlsen, B. Yang, X. Dong, Z. Wang, H. Liu, S. Wang, S. M. Zakeeruddin, A. Hagfeldt, M. I. Dar, X. Li and M. Grätzel, *Adv. Mater.*, 2020, **32**, 1907757.
22 L. Liang, H. Luo, J. Hu, H. Li and P. Gao, *Adv. Energy Mater.*, 2020, **10**, 2000197.
23 T. Yang, L. Mao, J. Shi, P. Zeng, F. Li, J. Gong, X. Huang, Z. Wang, W. Cui, D. Huang, H. Zhang, Y. Sun, X. Fang, Z. Liu, M. Liu and X. Cui, *Adv. Energy Mater.*, 2023, **14**, 2303149.
24 C. Liu, Y. Yang, H. Chen, J. Xu, A. Liu, A. S. R. Bati, H. Zhu, L. Grater, S. S. Hadke, C. Huang, V. K. Sangwan, T. Cai, D. Shin, L. X. Chen, M. C. Hersam, C. A. Mirkin, B. Chen, M. G. Kanatzidis and E. H. Sargent, *Science*, 2023, **382**, 810–815.
25 C. Li, X. Wang, E. Bi, F. Jiang, S. M. Park, Y. Li, L. Chen, Z. Wang, L. Zeng, H. Chen, Y. Liu, C. R. Grice, A. Abudulimu, J. Chung, Y. Xian, T. Zhu, H. Lai, B. Chen, R. J. Ellingson, F. Fu, D. S. Ginger, Z. Song, E. H. Sargent and Y. Yan, *Science*, 2023, **379**, 690–694.
26 B. Chen, J. Wang, N. Ren, P. Liu, X. Li, S. Wang, W. Han, Z. Zhu, J. Liu, Q. Huang, Y. Zhao and X. Zhao, *Interdiscip. Mater.*, 2023, **2**, 855–865.
27 Y. Ahmed, X. Feng, Y. Gao, Y. Ding, C. Long, M. Haider, H. Li, Z. Li, S. Huang, M. I. Saidaminov and J. Yang, *Acta Phys.-Chim. Sin.*, 2024, **40**, 2303057.
28 Q. Jiang, Y. Zhao, X. Zhang, X. Yang, Y. Chen, Z. Chu, Q. Ye, X. Li, Z. Yin and J. You, *Nat. Photonics*, 2019, **13**, 460–466.
29 M. Li, J. Zhou, L. Tan, Y. Liu, S. Wang, C. Jiang, H. Li, X. Zhao, X. Gao, W. Tress, L. Ding and C. Yi, *Energy Environ. Mater.*, 2022, **6**, 12360.
30 R. Lin, J. Xu, M. Wei, Y. Wang, Z. Qin, Z. Liu, J. Wu, K. Xiao, B. Chen, S. M. Park, G. Chen, H. R. Atapattu, K. R. Graham, J. Xu, J. Zhu, L. Li, C. Zhang, E. H. Sargent and H. Tan, *Nature*, 2022, **603**, 73–78.

31 L. Sibo, X. Xiaowei, W. Xin, H. Nuanshan, F. Jun, L. Dongxu, S. Yueyue, Z. Jia, K. Aung Ko Ko, H. Sisi and Q. Longbin, *Angew. Chem., Int. Ed.*, 2025, **64**, e202421174.

32 C. Ni, Y. Huang, T. Zeng, D. Chen, H. Chen, M. Wei, A. Johnston, A. H. Proppe, Z. Ning, E. H. Sargent, P. Hu and Z. Yang, *Angew. Chem., Int. Ed.*, 2020, **59**, 13977–13983.

33 B. Liu, H. Chen, J. Cao, X. Chen, J. Xie, Y. Shu, F. Yan, W. Huang and T. Qin, *Adv. Funct. Mater.*, 2023, **34**, 2310828.

34 Q. Jiang, Y. Zhao, X. Zhang, X. Yang, Y. Chen, Z. Chu, Q. Ye, X. Li, Z. Yin and J. You, *Nat. Photonics*, 2019, **13**, 460–466.

35 M. Yavari, M. Mazloum-Ardakani, S. Gholipour, M. M. Tavakoli, S.-H. Turren-Cruz, N. Taghavinia, M. Grätzel, A. Hagfeldt and M. Saliba, *Adv. Energy Mater.*, 2018, **8**, 1800177.

36 S. Luis, S. Maria, M. Nazario, J. M. Andrew, J. D. Trevor, R. Julius, S. Wolfgang and M. G. Dirk, *Angew. Chem., Int. Ed.*, 2006, **45**, 4637–4641.

37 F. Li, X. Deng, Z. Shi, S. Wu, Z. Zeng, D. Wang, Y. Li, F. Qi, Z. Zhang, Z. Yang, S.-H. Jang, F. R. Lin, S. W. Tsang, X.-K. Chen and A. K. Y. Jen, *Nat. Photonics*, 2023, **17**, 478–484.

38 H. Zhou, L. Yang, Y. Duan, M. Wu, Y. Li, D. Xu, H. Zou, J. Wang, S. Yang and Z. Liu, *Adv. Energy Mater.*, 2023, **13**, 2204372.

39 C. Zhang, H. Li, C. Gong, Q. Zhuang, J. Chen and Z. Zang, *Energy Environ. Sci.*, 2023, **16**, 3825–3836.

40 Y. Zhu, C. Li, J. Chen, Y. Zhang, J. Lu, M. Hu, W. Li, F. Huang, Y. B. Cheng, H. Park and S. Xiao, *Interdiscip. Mater.*, 2024, **3**, 369–379.

41 J. Liu, J. Chen, L. Xie, S. Yang, Y. Meng, M. Li, C. Xiao, J. Zhu, H. Do, J. Zhang, M. Yang and Z. Ge, *Angew. Chem., Int. Ed.*, 2024, **63**, 202403610.

42 S. Zhenhua, S. Kexuan, M. Yuanyuan, Z. Zewei, W. Yaohua, Z. Weifu, B. Yang, L. Xiaoyi, T. Ruijia, L. Chang and G. Ziyi, *Adv. Mater.*, 2024, **37**, 2410779.

43 T. S. Sherkar, C. Momblona, L. Gil-Escrig, J. Ávila, M. Sessolo, H. J. Bolink and L. J. A. Koster, *ACS Energy Lett.*, 2017, **2**, 1214–1222.

44 M. I. Saidaminov, J. Kim, A. Jain, R. Quintero-Bermudez, H. Tan, G. Long, F. Tan, A. Johnston, Y. Zhao, O. Voznyy and E. H. Sargent, *Nat. Energy*, 2018, **3**, 648–654.

45 D.-J. Xue, Y. Hou, S.-C. Liu, M. Wei, B. Chen, Z. Huang, Z. Li, B. Sun, A. H. Proppe, Y. Dong, M. I. Saidaminov, S. O. Kelley, J.-S. Hu and E. H. Sargent, *Nat. Commun.*, 2020, **11**, 1514.

46 C. H. Chen, F. Hu, Z. H. Su, Y. J. Yu, K. L. Wang, Y. R. Shi, J. Chen, Y. Xia, X. Y. Gao, Z. K. Wang and L. S. Liao, *Adv. Funct. Mater.*, 2023, **33**, 2213661.

47 C. Hao, T. Sam, C. Bin, H. Yi, G. Luke, Z. Tong, B. Koen, P. So Min, R. A. Harindi, G. Yajun, W. Mingyang, K. J. Andrew, Z. Qilin, X. Kaimin, Y. Danni, H. Congcong, C. Teng, J. Eui Hyuk, Z. Chun, Z. Wenjia, H. P. Andrew, H. Sjoerd, L. Frédéric, F. Tobin, R. G. Kenneth, N. Zhijun and H. S. Edward, *Nat. Photonics*, 2022, **16**, 352–358.

48 F. Dubecký, J. Ostwald, D. Kindl, P. Hubík, M. Dubecký, E. Gombia, A. Šagátová, P. Boháček, M. Sekáčová and V. Nečas, *Solid-State Electron.*, 2016, **118**, 30–35.

49 S. Ye, H. Rao, M. Feng, L. Xi, Z. Yen, D. H. L. Seng, Q. Xu, C. Boothroyd, B. Chen, Y. Guo, B. Wang, T. Salim, Q. Zhang, H. He, Y. Wang, X. Xiao, Y. M. Lam and T. C. Sum, *Nat. Energy*, 2023, **8**, 284–293.

50 J. Li, L. Xie, G. Liu, Z. Pu, X. Tong, S. Yang, M. Yang, J. Liu, J. Chen, Y. Meng, Y. Wang, T. Wang and Z. Ge, *Angew. Chem., Int. Ed.*, 2024, **63**, 202316898.

51 P. Zhu, D. Wang, Y. Zhang, Z. Liang, J. Li, J. Zeng, J. Zhang, Y. Xu, S. Wu, Z. Liu, X. Zhou, B. Hu, F. He, L. Zhang, X. Pan, X. Wang, N.-G. Park and B. Xu, *Science*, 2024, **383**, 524–531.

52 Z. Li, J. Dong, C. Liu, J. Guo, L. Shen and W. Guo, *Nano-Micro Lett.*, 2019, **11**, 50.

53 Y. Zheng, Y. Li, R. Zhuang, X. Wu, C. Tian, A. Sun, C. Chen, Y. Guo, Y. Hua, K. Meng, K. Wu and C.-C. Chen, *Energy Environ. Sci.*, 2023, **17**, 1153–1162.

54 X. Liu, Z. Yu, T. Wang, K. L. Chiu, F. Lin, H. Gong, L. Ding and Y. Cheng, *Adv. Energy Mater.*, 2020, **10**, 2001958.

55 J. Shi, J. Dong, S. Lv, Y. Xu, L. Zhu, J. Xiao, X. Xu, H. Wu, D. Li, Y. Luo and Q. Meng, *Appl. Phys. Lett.*, 2014, **104**, 063901.

56 W. Ke, G. Fang, J. Wan, H. Tao, Q. Liu, L. Xiong, P. Qin, J. Wang, H. Lei, G. Yang, M. Qin, X. Zhao and Y. Yan, *Nat. Commun.*, 2015, **6**, 6700.

57 S. Zhang, T. Tian, J. Li, Z. Su, C. Jin, J. Su, W. Li, Y. Yuan, J. Tong, Y. Peng, S. Bai, P. Müller-Buschbaum, F. Huang, Y. B. Cheng and T. Bu, *Adv. Funct. Mater.*, 2024, **34**, 2401945.